Unusual Structural and Spectroscopic Features of Some PNP-Pincer Complexes of Iron

Elizabeth M. Pelczar, Thomas J. Emge, Karsten Krogh-Jespersen,* and Alan S. Goldman*

Department of Chemistry and Chemical Biology, Rutgers−The State University of New Jersey, New Brunswick, New Jersey 08903

Received May 9, 2008

We report a structural, spectroscopic, and computational study of two $^{t\mathrm{Bu}}$PNP (2,6-bis(di-*tert*-butylphosphinomethyl)pyridine) complexes of iron, ($^{t\mathrm{Bu}}$PNP)$FeCl_2$ (**1**) and ($^{t\mathrm{Bu}}$PNP)$Fe(CO)_2$ (**3**). Complex **1**, ($^{t\mathrm{Bu}}$PNP)$FeCl_2$, also independently synthesized by Milstein, has unusually long iron−ligand bond distances. DFT calculations show that these are clearly attributable to its high-spin electronic structure, and in particular to occupancy of the strongly antibonding $d_{x^2-y^2}$ orbital. The crystal structure of **3** reveals two unusual aspects. (1) The geometry around the iron atom in **3** is much closer to square pyramidal (SQP; apical CO) than to trigonal bipyramidal (TBP), although five-coordinate Fe(0) complexes are generally expected to be TBP; moreover, Chirik et al. have reported that ($^{i\mathrm{Pr}}$PNP)$Fe(CO)_2$ has essentially a perfect TBP structure ($^{i\mathrm{Pr}}$PNP = 2,6-bis(di-isopropyl-phosphinomethyl)pyridine). (2) The apical carbonyl ligand in **3** deviates significantly from linearity (Fe−C−O = 171.9°). Additionally, complex **3** is intensely blue in color, which is unusual for an Fe(0) complex and also significantly different from the red color of Chirik's ($^{i\mathrm{Pr}}$PNP)$Fe(CO)_2$ species. Results from DFT calculations reproduce and explain these structural and spectroscopic aspects as well as the contrast between **3** and its $^{i\mathrm{Pr}}$PNP analogue.

1. Introduction

Pincer-ligated transition metal complexes are currently a subject of intense interest. Among the many applications of such species, (PCP)Ir complexes have demonstrated high efficacy as dehydrogenation catalysts.[1] In this context, we and others have begun to explore the chemistry of the isoelectronic PNP complexes of group 8 metals, including iron. Such complexes are also of great interest in the context of the high catalytic activity of iron complexes with mer-coordinating tridentate ligands, as reported by Brookhart[2] and then Gibson.[3] "Pincer"-ligated iron catalysts have seen other important catalytic applications as well.[4−9]

Scheme 1. Reaction Yielding ($^{t\mathrm{Bu}}$PNP)$FeCl_2$, 1

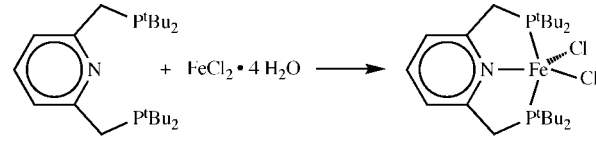

Our strategy in this regard was to synthesize a $^{\mathrm{R}}$PNP complex of iron ($^{\mathrm{R}}$PNP = κ^3-C_5NH_3-2,6-$(CH_2PR_2)_2$), in particular ($^{t\mathrm{Bu}}$PNP)$FeCl_2$ (**1**), and then reduce it to a precursor of zerovalent "($^{t\mathrm{Bu}}$PNP)Fe", the analogue of the catalytically active species "($^{t\mathrm{Bu}}$PCP)Ir". Although we have not in fact successfully generated such a species, in the course of reducing **1** we obtained the carbonyl complex ($^{t\mathrm{Bu}}$PNP)$Fe(CO)_2$ (**3**). This complex is found to have unusual spectroscopic and structural features; we address these, as well as interesting structural and electronic characteristics of complex **1**, through the use of DFT calculations.

2. Results and Discussion

2.1. ($^{t\mathrm{Bu}}$PNP)$FeCl_2$ (1). Sacco[10] and Nelson[11] have synthesized numerous ($^{\mathrm{Ph}}$PNP)FeX_2 (X = Cl, Br, I, NCS, NO_3) complexes; these and related complexes have been investigated for polymerization activity by Rieger.[12] Following a method similar to that used by Sacco[10] to synthesize ($^{\mathrm{Ph}}$PNP)$Fe(NO_3)_2$,

* Corresponding authors. E-mail: alan.goldman@rutgers.edu; kroghjes@rutgers.edu.

(1) (a) Gupta, M.; Hagen, C.; Flesher, R. J.; Kaska, W. C.; Jensen, C. M. *Chem. Commun.* **1996**, 2083–2084. (b) Xu, W.; Rosini, G. P.; Gupta, M.; Jensen, C. M.; Kaska, W. C.; Krogh-Jespersen, K.; Goldman, A. S. *Chem. Commun.* **1997**, 2273–2274. (c) Liu, F.; Pak, E. B.; Singh, B.; Jensen, C. M.; Goldman, A. S. *J. Am. Chem. Soc.* **1999**, *121*, 4086–4087.

(2) (a) Small, B. L.; Brookhart, M.; Bennett, A. M. A. *J. Am. Chem. Soc.* **1998**, *120*, 4049–4050. (b) Small, B. L.; Brookhart, M. *J. Am. Chem. Soc.* **1998**, *120*, 7143–7144. (c) Bennett, A. M. A.; Small, B. L.; Brookhart, M. S. In Book of Abstracts; 215th ACS National Meeting, Dallas, March 29−April 2, 1998; , PMSE-038. (d) Small, B. L.; Brookhart, M. *Macromolecules* **1999**, *32*, 2120–2130.

(3) (a) Britovsek, G.; Gibson, V. C.; Kimberley, B. S.; Maddox, P. J.; Mctavish, S. J.; Solan, G. A.; White, A. J. P.; Williams, D. J. *Chem. Commun.* **1998**, 849–850. (b) Britovsek, G. J. P.; Bruce, M.; Gibson, V. C.; Kimberley, B. S.; Maddox, P. J.; Mastroianni, S.; McTavish, S. J.; Redshaw, C.; Solan, G. A.; Stroemberg, S.; White, A. J. P.; Williams, D. J. *J. Am. Chem. Soc.* **1999**, *121*, 8728–8740.

(4) Bart, S. C.; Lobkovsky, E.; Chirik, P. J. *J. Am. Chem. Soc.* **2004**, *126*, 13794–13807.

(5) Bouwkamp, M. W.; Lobkovsky, E.; Chirik, P. J. *J. Am. Chem. Soc.* **2005**, *127*, 9660–9661.

(6) Bart, S. C.; Chlopek, K.; Bill, E.; Bouwkamp, M. W.; Lobkovsky, E.; Neese, F.; Wieghardt, K.; Chirik, P. J. *J. Am. Chem. Soc.* **2006**, *128*, 13901–13912.

(7) Hoelscher, M.; Prechtl, M. H. G.; Leitner, W. *Chem.−Eur. J.* **2007**, *13*, 6636–6643.

(8) Benito-Garagorri, D.; Wiedermann, J.; Pollak, M.; Mereiter, K.; Kirchner, K. *Organometallics* **2007**, *26*, 217–222.

(9) Benito-Garagorri, D.; Becker, E.; Wiedermann, J.; Lackner, W.; Pollak, M.; Mereiter, K.; Kisala, J.; Kirchner, K. *Organometallics* **2006**, *25*, 1900–1913.

(10) Giannoccaro, P.; Vasapollo, G.; Nobile, C. F.; Sacco, A. *Inorg. Chim. Acta* **1982**, *61*, 69–75.

(11) Nelson, S. M.; Dahlhoff, W. V. *J. Chem. Soc. (A)* **1971**, 2184–2190.

(12) Muller, G.; Klinga, M.; Leskela, M.; Rieger, B. *Z. Anorg. Allg. Chem.* **2002**, *628*, 2839–2846.

10.1021/om800425p CCC: $40.75
Publication on Web 10/17/2008

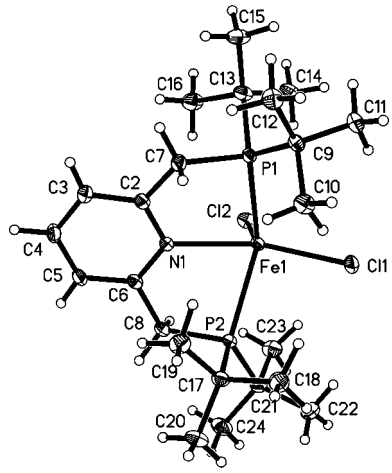

Figure 1. Crystal structure of ($^{t\text{Bu}}$PNP)$FeCl_2$, **1**.

Table 1. Crystal Data and Structure Refinement for ($^{t\text{Bu}}$PNP)$FeCl_2$ (1) and ($^{t\text{Bu}}$PNP)$Fe(CO)_2$ (3)

empirical formula	$C_{23}H_{43}Cl_2FeNP_2$	$C_{25}H_{43}FeNO_2P$
fw	522.27	507.39
temperature	100(2) K	100(2) K
wavelength	0.71073 Å	0.71073 Å
cryst syst	monoclinic	orthorhombic
space group	$P2_1/n$	$P2_12_12_1$
a	12.0831(9) Å	11.7404(12) Å
b	15.5084(12) Å	14.5944(14) Å
c	14.504 9(11) Å	15.3327(15) Å
α	90°	90°
β	91.093(2)°	90°
γ	90°	90°
volume	2717.6(4) Å^3	2627.2 Å^3
Z	4	4
absorp coeff	0.880 mm^{-1}	0.717 mm^{-1}
goodness-of-fit on F^2	1.012	1.041
final *R* indices [$I > 2\sigma(I)$]	R1 = 0.0349 wR2 = 0.0753	R1 = 0.0219 wR2 = 0.561

$FeCl_2 \cdot 4H_2O$ in ethanol was added to a suspension of $^{t\text{Bu}}$PNP ligand in benzene (Scheme 1). Complex **1** precipitated as a yellow crystalline solid. Crystals suitable for X-ray diffraction were obtained by recrystallization from cold methanol (Figure 1).[13] During the course of this work ($^{t\text{Bu}}$PNP)$FeCl_2$ was also independently synthesized and crystallographically characterized by Milstein.[14]

Complex **1** is found to have a distorted square-pyramidal structure with a chloride in the apical position. The iron−ligand bond distances are all quite long; in particular an unusually long Fe−N bond length of 2.329 Å (Table 2) is noteworthy. For comparison, the 2,6-bis[1-(2,6-diisopropylphenylimino)ethyl]pyridineiron(II) chloride ((NNN)$FeCl_2$) species reported by Brookhart features a much shorter Fe−N bond of 2.091(4) Å,[2,3] and related complexes reported by Brookhart[2] and Gibson[3] show similarly short Fe−N bonds.

Table 2. Selected Bond Lengths and Angles for ($^{t\text{Bu}}$PNP)$FeCl_2$, 1; X-ray Structure and Calculated Quintet, Triplet, and Singlet States

	X-ray	calc, $S = 2$	calc, $S = 1$	calc, $S = 0$
	Bond Lengths (Å)			
Fe(1)−N(1)	2.3286(13)	2.363	1.997	1.955
Fe(1)−Cl(1)	2.3816(5)	2.319	2.277	2.286
Fe(1)−Cl(2)	2.3028(5)	2.317	2.375	2.290
Fe(1)−P(1)	2.5149(5)	2.518	2.347	2.314
Fe(1)−P(2)	2.5168(5)	2.507	2.331	2.269
	Bond Angles (deg)			
Cl(1)−Fe(1)−N(1)	153.95(3)	157.8	168.2	169.8
Cl(2)−Fe(1)−N(1)	97.61(3)	86.2	87.8	86.7
Cl(1)−Fe(1)−Cl(2)	107.628(17)	115.9	103.8	103.2
N(1)−Fe(1)−P(1)	77.13(3)	76.5	84.4	86.0
N(1)−Fe(1)−P(2)	73.59(3)	75.2	82.4	85.4
Cl(1)−Fe(1)−P(1)	101.249(16)	95.6	93.9	95.1
Cl(1)−Fe(1)−P(2)	93.402(16)	98.9	93.8	91.4
Cl(2)−Fe(1)−P(1)	106.190(16)	108.8	106.8	98.1
Cl(2)−Fe(1)−P(2)	104.774(16)	99.8	98.3	92.8
P(1)−Fe(1)−P(2)	139.582(16)	137.9	151.1	165.7

Magnetic susceptibility measurements show that **1** is a high-spin, d^6 Fe(II) complex. The experimental value obtained for the effective magnetic moment of **1** is $\mu_{\text{eff}} = 5.14\ \mu_B$, in agreement with the value reported by Milstein (5.3 μ_B) and consistent with the idealized theoretical value of 4.90 μ_B representing a quintet spin state ($S = 2$, four unpaired electrons). The NMR spectral properties of **1** reflected its paramagnetism. The $^{31}P\{^1H\}$ NMR showed no signals. Broad peaks in the ^1H NMR spectrum (δ −10.0 to 54.9) could, however, be assigned on the basis of their integral values (see Experimental Section).

The electronic structural properties of **1** were computed from first-principles electronic structure calculations based on DFT (see Computational Details). Quintet, as well as triplet and singlet, spin states were investigated, and structural minima corresponding to both trigonal-bipyramidal (**1-TBP**, C_2 symmetry) and square-planar (**1-SQP**, C_1 symmetry) coordination geometries were located on the potential energy surface. In full accord with the results of the magnetic susceptibility measurements described above and the X-ray structural determination, the ground state is calculated to be quintet **1-SQP**; the triplet and singlet states in **1-SQP** are computed to be 8.3 and 19.9 kcal/mol, respectively, higher in free energy.[15] The quintet state of **1-TBP** is calculated to be only 1.3 kcal/mol above quintet **1-SQP** in free energy ($\Delta H = 0.4$ kcal/mol), illustrating the flatness of the potential energy surface with respect to motion of the Cl ligands in the $NFeCl_2$ plane. Interestingly, when sterically less demanding Me rather than *t*-Bu groups were applied as substituents on phosphorus, the computations could locate only a TBP structure.

The computed Fe−N distance (Table 2) in quintet **1-SQP** is indeed long at 2.363 Å (and even longer for the higher-energy quintet **1-TBP** isomer, at 2.414 Å) and matches well the crystallographic Fe−N bond length of 2.329 Å. Likewise, the Fe−P distances are long, with calculated and crystallographic average values for **1-SQP** at 2.513 and 2.516 Å, respectively. Generally, the metrics of the experimental and computed structures for **1** compare well, with the largest discrepancies involving the two Cl ligands. The asymmetry in Cl bond lengths is larger in the experimental structure; for example, computed

(13) (a) Pelczar, E. M.; Goldman, A. S. In Abstracts of Papers, 226th ACS National Meeting, New York, 2003, INOR-438. (b) Pelczar, E. M.; Goldman, A. S. Abstracts of Papers, 228th ACS National Meeting, Philadelphia, 2004, INOR-222(c) Pelczar, E. M.; Emge, T. J.; Goldman, A. S. *Abstracts*; 37th Middle Atlantic Regional Meeting of the American Chemical Society, New Brunswick, NJ, May 22−25, 2005, GENE-151.

(14) Zhang, J.; Gandelman, M.; Herrman, D.; Leitus, G.; Shimon, L. J. W.; Ben-David, Y.; Milstein, D. *Inorg. Chim. Acta* **2006**, *359*, 1955–1960. Note that ($^{t\text{Bu}}$PNP)$FeCl_2$ was crystallized in this work in a different space group ($P\bar{1}$). Bond distances and angles obtained from this study were very similar to those obtained in the present work (corresponding bond distances equal within 0.03 Å; angles around Fe equal within 6°), suggesting that packing forces do not play a critical role in determining the molecular geometry.

(15) The triplet and singlet states are probably even higher in energy, since DFT with standard GGA exchange−correlation functionals (such as the PBE functionals used here) are known to underestimate the relative stability of high-spin states in Fe complexes, cf.: Swart, M.; Groenhof, A. R.; Ehlers, A. W.; Lammertsma, K. *J. Phys. Chem.* **2004**, *108*, 5479–5483.

Fe−Cl(1) and Fe−Cl(2) bond lengths are 2.319 and 2.317 Å, but 2.382 and 2.303 Å experimentally.[16]

The computed Fe−N bond length for the three spin states of **1-SQP** shows an interesting trend: exceedingly short in the singlet (1.96 Å), only slightly longer in the triplet (2.00 Å), and substantially longer at 2.36 Å in the quintet state. For the Fe−P distances the trend is similar (average value): 2.29 Å (S), 2.34 Å (T), and 2.51 Å (Q). These trends are well rationalized when small modifications are applied to the simple MO diagram for an idealized AB_5 square-pyramidal complex.[17] The approximate orbital ordering in **1-SQP** is $d_{xy} < d_{xz} \sim d_{yz} < d_{z^2} < d_{x^2-y^2}$ (z axis defined by the apical Fe−Cl(2) bond). In the singlet, the three Fe d(π)-type orbitals (d_{xy}, d_{xz}, d_{yz}) are all doubly occupied; these orbitals are π antibonding with respect to the ligands. The d_{z^2} orbital is only slightly σ antibonding with respect to the four basal ligands, whereas the $d_{x^2-y^2}$ orbital is strongly σ antibonding with respect to these ligands. The d_{z^2} orbital becomes singly occupied in the triplet, and in the quintet state both the d_{z^2} and the $d_{x^2-y^2}$ orbitals are singly occupied (as are the d_{xz} and d_{yz} orbitals). Hence, a general elongation of Fe−N and Fe−P bonds is computed for the higher spin multiplicity states as the population in the σ antibonding orbitals increases. The bond length changes are much smaller for the fourth basal ligand, Cl(1), although the Fe−Cl(1) distance is longest in quintet **1-SQP**. The smaller Fe−Cl(1) bond length variations can be rationalized by noting that the partial occupation of the σ antibonding orbitals is offset by the corresponding removal of electrons from the π antibonding orbitals.

In the case of the apical ligand, Cl(2), only the d_{z^2} orbital is significantly σ antibonding; accordingly, a large increase in Fe−Cl(2) bond length (~0.09 Å) is calculated in the triplet relative to the singlet state. In contrast to the basal ligands, the $d_{x^2-y^2}$ orbital is not antibonding with respect to Cl(2); hence the single occupancy of $d_{x^2-y^2}$ introduced in the quintet does not result in an increase in the Fe−Cl(2) bond length, relative to the triplet. Indeed, removal of an electron from the π antibonding orbitals (d_{xz}, d_{yz}) affords a calculated *decrease* in this bond length (from 2.38 Å to 2.32 Å), in sharp contrast with the increased bond lengths observed for the basal ligands in the quintet state (Table 2).

The computed difference in Fe−N bond length between quintet and triplet states is almost 0.4 Å, twice the analogous change in the Fe−P bond lengths. We attribute this result to a combination of two factors. One is the direct weakening of the Fe−N bond discussed above, reflecting the strongly antibonding nature of the partially occupied $d_{x^2-y^2}$ orbital. There is also an indirect weakening of the Fe−N bond arising from geometrical constraints. The P−Fe−P angle is strongly acute (~140°) in **1**, and the PNP framework is semirigid; consequently, if the Fe−P distances increase, so must the Fe−N distance.

2.2. [($^{t\mathrm{Bu}}$PNP)FeHCl] (2). Addition of 4 equiv of NEt_4BH_4 to an acetonitrile solution of **1**, at room temperature, effectuated a color change from yellow to bright red. The ^{1}H NMR spectrum showed the presence of a new triplet with a chemical shift of δ −13.6 ppm, consistent with the formation of a hydride complex. The selectively decoupled ^{31}P NMR showed a doublet centered at 102.7 ppm, consistent with two equivalent phosphorus atoms coupling with one hydride. The color change is probably

Scheme 2. Synthesis of ($^{t\mathrm{Bu}}$PNP)FeHCl, 2, or possible adduct thereof

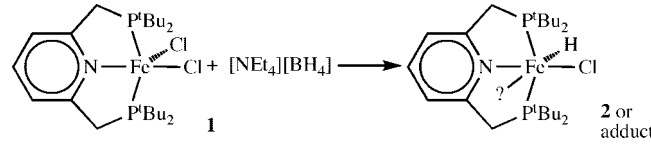

Scheme 3. Synthesis of ($^{t\mathrm{Bu}}$PNP)Fe(CO)$_2$ (3)

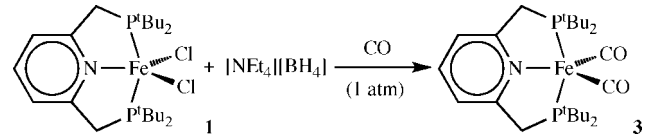

associated with the formation (Scheme 2) of ($^{t\mathrm{Bu}}$PNP)FeHCl (**2**) or a complex thereof, perhaps ($^{t\mathrm{Bu}}$PNP)FeHCl(NCMe). Attempts to isolate **2** for X-ray diffraction and elemental analysis resulted in decomposition of the complex.

Our calculations indicate that **2** (like **1**) should adopt a SQP structure (H apical) but possess a singlet ground state. The triplet and quintet states for **2** are computed 7.6 and 10.8 kcal/mol, respectively, above the singlet state in free energy. Adduct formation of **2** with MeCN is computed to be moderately favorable, $\Delta G = -2.5$ kcal/mol.

2.3. ($^{t\mathrm{Bu}}$PNP)Fe(CO)$_2$ (3). 2.3.1. Synthesis and Experimental Characterization. In an attempt to trap the putative complex ($^{t\mathrm{Bu}}$PNP)FeHCl, the reduction of **1** by NEt_4BH_4 was conducted under 1 atm of CO (Scheme 3). Rather than obtaining the target complex ($^{t\mathrm{Bu}}$PNP)FeHCl(CO), however, the resulting product was ($^{t\mathrm{Bu}}$PNP)Fe(CO)$_2$ (**3**). Blue crystals of **3** were obtained by slow evaporation of acetonitrile, and the structure was determined by X-ray crystallography (Figure 2).[13]

Two structural features of complex **3** are noteworthy. First, the coordination geometry around iron is much closer to a SQP geometry (conveyed in figure) than to the TBP geometry, which is expected of low-spin Fe(0).[18,19] The angles C(25)−Fe(1)−C(24), C(25)−Fe(1)−N(1), C(25)−Fe(1)−P(2), and C(25)−Fe(1)−P(1) (Figure 2) would approach 120°, 120°, 90°, and 90°, respectively, in approaching the limit of an idealized TBP geometry (assuming the phosphino groups would occupy the apical positions). The observed values for these angles are, respectively, 105.8°, 101.6°, 101.9°, and 103.4°. Several parameters can be used to quantify the degree to which a structure approaches SQP. Perhaps the one most suitable to a complex containing a ligand such as PNP, in which the N−M−P angles are constrained to be significantly less than 90°, is based on the $L_{apical}-M-L_{basal}$ angles, which are all equal in the ideal SQP geometry. Thus, for example, Nardelli et al. note that the geometry of $Fe(CO)_3(L_2)$ species is closer to SQP than to TBP; this is based in part on the observation that the average deviation of the angles $L_{apical}-M-L_{basal}$ from their mean value is 5.4° and 7.1° for $L_2 = Ph_2PCH_2CH_2PPh_2$ and $L_2 = Ph_2PCH_2PPh_2$, respectively.[20] In the case of complex **3** the average deviation from the mean is only 1.4°. The SQP geometry is conveyed.

The second structural feature of interest is that the CO ligand occupying the apical position of the quasi-SQP deviates significantly from linearity (Fe−C−O = 171.87(10)°). The other

(16) Interestingly, in a constrained geometry optimization in which the Fe−Cl bond lengths and N−Fe−Cl bond angles were held at the values experimentally observed, the optimized Fe−N value for quintet **1-SQP** is 2.350 Å, extremely close to the experimental value of 2.329 Å.

(17) Albright, T. A.; Burdett, J. K.; Whangbo, M. Orbital Interactions in Chemistry; John Wiley & Sons: New York, 1985.

(18) See: Casey, C. P.; Whiteker, G. T.; Campana, C. F.; Powell, D. R *Inorg. Chem.* **1990**, *29*, 3376–3381, and references therein.

(19) For an example of a square-pyramidal high-spin Fe(0) complex, see ref 4 and references therein.

(20) Battaglia, L. P.; Delledonne, D.; Nardelli, M.; Pelizzi, C.; Predieri, G. *J. Organomet. Chem.* **1987**, *330*, 101–113.

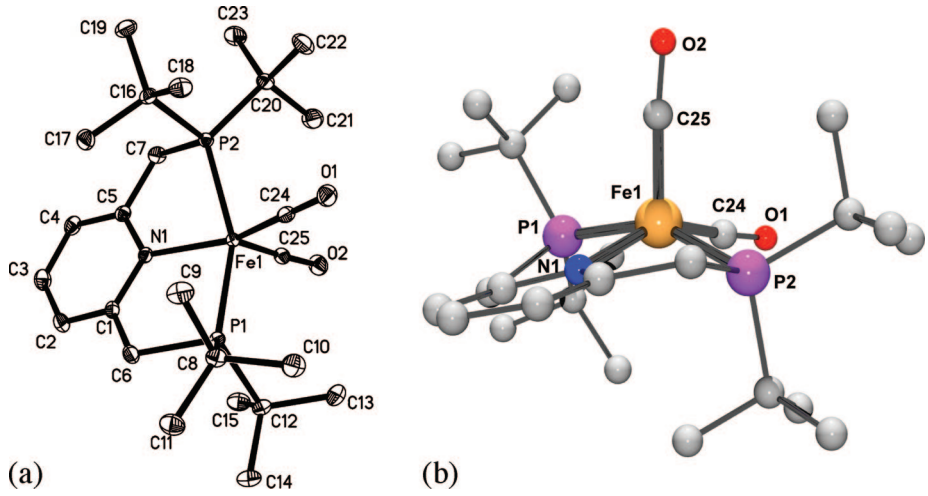

Figure 2. (a) ORTEP diagram of the structure of ($^{t\text{Bu}}$PNP)Fe(CO)$_2$ (**3**). (b) POV-Ray diagram (oriented to emphasize the SQP geometry).

Table 3. Selected Bond Lengths and Angles of ($^{t\text{Bu}}$PNP)Fe(CO)$_2$, 3, and Calculated Values for 3-SQP and 3-TBP

	X-ray	calc (**3-SQP**)	calc (**3-TBP**)
	Bond Lengths (Å)		
Fe(1)−N(1)	2.0503(9)	2.027	2.044
Fe(1)−C(24), basal[a]	1.7310(12)	1.727	1.735
Fe(1)−C(25), apical[a]	1.7708(12)	1.754	
Fe(1)−P(1)	2.2322(3)	2.251	2.253
Fe(1)−P(2)	2.2066(4)	2.236	
	Bond Angles (deg)		
O(1)−C(24)−Fe(1)	176.68(10)	176.2	171.0
O(2)−C(25)−Fe(1)	171.87(10)	173.9	171.0
C(24)−Fe(1)−C(25)	105.78(5)	102.7	106.6
C(24)−Fe(1)−N(1)	152.52(5)	158.4	126.7
C(25)−Fe(1)−N(1)	101.57(4)	98.8	126.7
C(24)−Fe(1)−P(2)	90.13(4)	91.2	93.7
C(25)−Fe(1)−P(2)	101.94(4)	101.2	95.9
N(1)−Fe(1)−P(1)	84.04(3)	84.9	81.9
N(1)−Fe(1)−P(2)	81.55(3)	82.5	81.9
C(24)−Fe(1)−P(1)	92.21(4)	91.7	93.7
C(25)−Fe(1)−P(1)	103.35(4)	104.5	95.9
P(1)−Fe(1)−P(2)	152.917(13)	152.8	163.9

[a] The terms "basal" and "apical" refer only to **3** (X-ray) and **3-SQP**.

carbonyl (in the "SQP basal plane") is also bonded in a nonlinear fashion but significantly less so (Fe−C−O = 176.68(10)°).

The spectroscopic properties of **3** are also unusual. We note the bright blue color in both solution and in the solid state (including the crystal used for structural determination). Fe(0) complexes are typically yellow,[21−24] and none to our knowledge have been reported as blue. The color of **3** arises from an electronic absorption band peaking at λ_{max} = 627 nm in acetonitrile solvent.

The ^{31}P{^{1}H} NMR spectrum (toluene-d_8 solvent) gives a broad signal at δ 120 ppm, which is sharpened at −80 °C. ^{1}H NMR signals are broad even at −80 °C. On the basis of the crystal structure it might be expected that the *tert*-butyl and methylene proton signals would be broadened by inequivalence. However even the aryl proton signals are broad, and even at −80 °C.

($^{t\text{Bu}}$PNP)Fe(^{13}CO)$_2$ (**3-^{13}CO**) was synthesized under ^{13}CO atmosphere; its ^{13}C NMR spectrum showed a triplet at δ 230.65 ppm. The ^{31}P NMR spectrum of **3-^{13}CO** was also a triplet, confirming the presence of two CO ligands in the complex. Thus if **3** were to maintain a SQP geometry in solution, the CO ligands are rapidly exchanging on the NMR time scale. Note that when unlabeled **3** was placed under an atmosphere of ^{13}CO, no incorporation of isotopically labeled CO was observed, as monitored by either ^{13}C or ^{31}P NMR spectroscopy.

Unexpectedly, the infrared spectrum of **3** (THF solvent) shows four bands in the carbonyl region (see Supporting Information): two strong bands at 1870 and 1819 cm^{-1} and two weaker bands/shoulders (each overlapping with the neighboring stronger band to the blue) at 1846 and 1797 cm^{-1}. The IR spectrum of **3-^{13}CO** shows the same pattern with the bands all shifted approximately by the reduced mass ratio factor of ∼0.9778: strong bands at 1828 and 1775 cm^{-1} along with weaker bands at 1804 and 1756 cm^{-1}, thus confirming the ν_{CO} assignment. Obviously, the presence of four ν_{CO} bands is not consistent with a single dicarbonyl structure.

During the course of this work the Chirik group independently reported the synthesis and structural characterization of ($^{i\text{Pr}}$PNP)Fe(CO)$_2$ (**4**).[25] Superficially, **3** and **4** would appear to be close analogues, differing only in the ornamentation on their respective PNP skeletons. However, the crystal structure of **4** reveals that its coordination geometry shows no relationship to that of **3**. Rather, the angles in the plane of Fe, N, and the carbonyl C atoms are all remarkably close to that of an ideal TBP structure: 120 ± 0.1°. Notably, however, the Fe−C−O angles in **4** are nonlinear, 174.84(11)°, although not as bent as observed for the apical CO in **3**. Furthermore, complex **4** is reported to be red in the solid state, whereas **3** forms a bright blue complex. And while the IR spectrum of **3** has four ν_{CO} bands, that of **4** has just two such bands, at 1842 and 1794 cm^{-1}, which are, interestingly, very close to the two weaker bands in the spectrum of **3** at 1846 and 1797 cm^{-1}.[25]

The Chirik group has also reported an iron(0) bis(dinitrogen) complex bearing a pincer-type (NNN) pyridinediimine ligand, ($^{i\text{Pr}}$PDI)Fe(N$_2$)$_2$ (**5**; $^{i\text{Pr}}$PDI = [(2,6-*i*-Pr)$_2$C$_6$H$_3$N=CMe]$_2$C$_5$H$_3$N).[4] The $^{i\text{Pr}}$PDI ligand is obviously much less closely related to $^{t\text{Bu}}$PNP than is $^{i\text{Pr}}$PNP; moreover, complex **5** is high spin, unlike

(21) Birk, R.; Berke, H.; Hund, H.-U.; Huttner, G.; Zsolnai, L.; Dahlenburg, L.; Behrens, U.; Sielisch, T. *J. Organomet. Chem.* **1989**, *372*, 397–410.
(22) Hanson, A. W. *Acta Crystallogr.* **1962**, *15*, 930–933.
(23) Vancheesan, S. *Indian J. Chem.* **1982**, *21A*, 579–582.
(24) Braunstein, P.; Clerc, G.; Morise, X. *New J. Chem.* **2003**, *27*, 68–72.
(25) Trovitch, R. J.; Lobkovsky, E.; Chirik, P. J. *Inorg. Chem.* **2006**, *45*, 7252–7260.

Table 4. Comparison of Selected Bond Lengths and Angles of ($^{t\text{Bu}}$PNP)Fe(CO)$_2$ (3)[a] and ($^{i\text{Pr}}$PNP)Fe(CO)$_2$ (4)[b]

		calculated (DFT)			
	3, X-ray	**3-SQP**	**3-TBP**	**4**	**4**, X-ray[b]
		Bond Lengths[a] (Å)			
Fe−N	2.0503(9)	2.027	2.044	2.036	2.0684(8)
Fe−C (basal)	1.7310(12)	1.727	1.735	1.742	1.7325(9)
Fe−C (apical)	1.7708(12)	1.754			
Fe−P	2.2322(3)	2.236	2.253	2.209	2.1941(2)
Fe−P	2.20766(4)	2.251			
		Bond Angles[a] (deg)			
Fe−C−O (basal)	176.68(10)	176.2	171.0	174.6	174.84(11)
Fe−C−O (apical)	171.87(10)	173.9			
C−Fe−C	105.78(5)	102.7	106.6	115.0	119.91(7)
C(basal)−Fe−N	152.52(5)	158.4	126.7	122.5	120.04(3)
C(apical)−Fe−N	101.57(4)	98.8			
C(basal)−Fe−P	90.13(4)	91.7, 91.2	93.7, 95.9	91.6, 95.5	91.83(3)
C(apical)−Fe−P	101.94(4)	101.2, 104.5			

[a] The terms "basal" and "apical" refer only to **3** (X-ray) and **3-SQP**. [b] Ref 25.

Table 5. Calculated and Experimental Infrared Spectral (ν_{CO}) Data for (^{R}PNP)Fe(CO)$_2$

	ν_{CO} (cm^{-1}) experimental	ν_{13CO} (cm^{-1}) predicted from ν_{12CO} (cm^{-1})[a]	ν_{CO} (cm^{-1}) DFT "THF"	ν_{CO} (cm^{-1}) DFT gas phase
($^{t\text{Bu}}$PNP)Fe(CO)$_2$ SQP	1870, 1819		1875, 1830	1892, 1856
($^{t\text{Bu}}$PNP)Fe(^{13}CO)$_2$ SQP	1828, 1775	1828, 1779	1830, 1786	1846, 1811
($^{t\text{Bu}}$PNP)Fe(CO)$_2$ TBP	1846, 1797		1852, 1809	1869, 1835
($^{t\text{Bu}}$PNP)Fe(^{13}CO)$_2$ TBP	1804, 1756	1805, 1757	1807, 1765	1823, 1790
($^{i\text{Pr}}$PNP)Fe(CO)$_2$ TBP	1842, 1794[b]		1864, 1816	1882, 1847

[a] Computed from the ratio of ^{13}CO/^{12}CO reduced masses. [b] Ref 25.

either **3** or **4**. Thus it is quite remarkable that the structure of the bis(dinitrogen) complex is strikingly similar to that of dicarbonyl complex **3**. The coordination geometry of **5**, like that of **3**, is square pyramidal: (N(basal-N$_2$)−Fe−N(apical-N$_2$) = 98.0°, N(basal-N$_2$)−Fe−N(pyridine) = 159.1°, N(pyridine)−Fe−N(apical-N$_2$) = 102.9°). Most remarkably, the Fe−N−N angle (apical N$_2$ ligand) in **5** is, within experimental error, equal to the Fe−C−O angle in **3** (171.81(17)° vs 171.87(10)° for **3**).

2.3.2. ($^{t\text{Bu}}$PNP)Fe(CO)$_2$ (3); Computational Results and Interpretation. DFT calculations prove extremely valuable in understanding the unusual properties of **3** and the differences between complexes **3** and **4**.

The global energy minimum calculated for ($^{t\text{Bu}}$PNP)Fe(CO)$_2$ is a singlet TBP structure (**3-TBP**) of C_2 symmetry (the atoms Fe−N−*p*-C(PNP) define the 2-fold rotation axis), in contrast with the crystallographically determined SQP structure of **3**. The calculated structure of **3-TBP** is, however, in good agreement with the structural parameters obtained by Chirik,[25] as well as our DFT-derived structure, for the $^{i\text{Pr}}$PNP analogue **4** (see Table 4 for some comparisons).

However, a second minimum with an approximately SQP geometry (**3-SQP**) and an energy only 1.0 kcal/mol above **3-TBP** was located as well. The geometry of **3-SQP** is in excellent agreement with the X-ray structure of **3** (Tables 3 and 4). For example, the N−Fe−C(apical), C−Fe−C, and N−Fe−C(basal) angles are calculated to be 98.8°, 102.7°, and 158.4°, respectively, as compared with respective measured angles of 101.6°, 105.8°, and 152.5°. The calculations also reproduce well the Fe−C−O angles and the greater length of the apical Fe−C vs the basal Fe−C bond (1.754 and 1.727 Å vs X-ray values of 1.771 and 1.731 Å). Thus, as the unusual structural aspects of **3** are well reproduced by gas-phase calculations, it is clear that they are not the result of crystal-packing effects.

The computed enthalpy difference between **3-TBP** and **3-SQP**, 0.4 kcal/mol, is even smaller than the potential energy difference and still favors **3-TBP**, but the calculated free energy of **3-SQP** is actually *lower*, by 0.6 kcal/mol, than that of **3-TBP**. Thus, the calculations predict two isomers of **3** that are nearly equal in free energy (idealized gas phase). Taking these free energies at face value, **3-SQP** should be the dominant isomer (~3:1 ratio at 25 °C), in accord with the SQP geometry observed in the X-ray structure; however, this agreement could certainly be fortuitous. The transition state for **3-TBP** ↔ **3-SQP** interconversion is computed only 1.6 kcal/mol above **3-SQP** (1.0 kcal/mol above **3-TBP**); thus, interconversion between the two isomers, and exchange between the inequivalent carbonyl ligands of **3-SQP**, is predicted to be very fast on the NMR time scale, in agreement with the observation of only one carbonyl peak in the ^{13}C NMR spectrum of **3-^{13}CO**.

The IR spectra (Table 5), measured in THF solution, provide much more quantitative support than the X-ray results for the computational prediction of nearly isoenergetic SQP and TBP isomers of **3**. The less intense set of IR bands for **3** is observed at 1846 and 1797 cm^{-1}, very close to the values measured for the TBP complex **4** (1842 and 1794 cm^{-1});[25] consequently, these two bands of **3** (in solution) can be attributed to the occurrence of the minor isomer, **3-TBP**. Calculations support this assignment with (unscaled) ν_{CO} values of 1852 and 1809 cm^{-1} predicted for **3-TBP** (in THF). The conclusion, that the major isomer in solution has the crystallographically observed SQP geometry, is also strongly supported by the frequency calculations for **3-SQP**: ν_{CO} values of 1875 and 1830 cm^{-1} as compared with experimental values of 1870 and 1819 cm^{-1}.

We could locate only a TBP structure for the ($^{i\text{Pr}}$PNP)Fe(CO)$_2$ complex **4**; all attempts at generating a SQP-type potential energy minimum inevitably reverted to TBP upon geometry optimization. The fact that **4** clearly possesses a TBP geometry, while **3** is SQP (in the crystal and as the major isomer in solution), strongly suggests that the origin of this difference is based in differential steric interactions. A priori, it might be unclear why increased bulk of the phosphinoalkyl groups in **3** would favor the SQP relative to the TBP geometry; however,

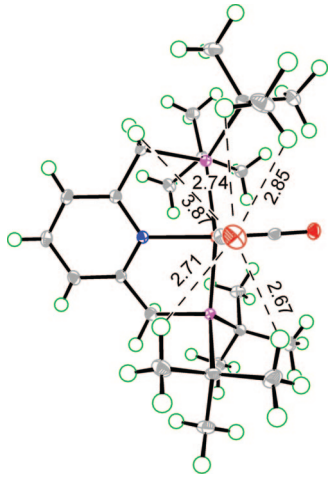

Figure 3. Crystal structure of **3**, showing interaction distances (in Å) between select ^{t}Bu hydrogen atoms and the carbonyl groups.

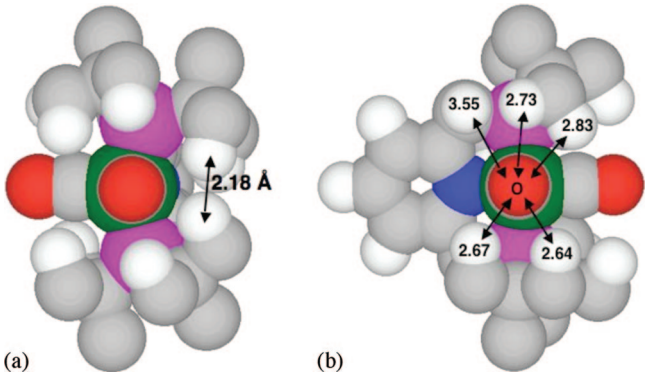

Figure 4. DFT structures of **3-SQP** with selected H's shown to illustrate crowding; others omitted for clarity. (a) Viewed down the O−C axis of the basal carbonyl, revealing relatively close contact between *tert*-butyl ligands on the two phosphino groups. (b) Viewed down the O−C axis of the apical carbonyl, with H−O(carbonyl) distances shown (Å). (See Figure 3 for comparison with crystallographic values.)

examination of either crystal or DFT structures reveals the origin of this steric effect. Even a ligand as small as CO encounters steric resistance from the bulky phosphino-*tert*-butyl groups. Viewed down the O−C axis of the basal carbonyl (Figure 4a), we note that the presence of a full vacant site trans to the apical CO ligand allows the phosphino groups to bend away from the apical CO. Indeed, this effect is so pronounced that *tert*-butyl groups of the two (nominally trans) phosphino groups are within van der Waals contact of each other: on the side opposite the apical CO, one of the H−H distances (between ^{t}Bu$_2$P groups) is only 2.18 Å in **3-SQP**.

Thus, the origin of the unusual SQP coordination geometry of **3** is apparently found in differential steric interactions. The second unusual feature however, the slightly bent CO angle, does *not* appear to be attributable to steric factors. Viewed down the O−C axis of the apical carbonyl (Figure 4b), we see that this carbonyl is flanked quite symmetrically by C−H bonds and the carbonyl oxygen does not appear to be "pushed" in any particular direction; no contacts are observed shorter than the van der Waals distance of 2.6 Å. Indeed, the bending of the apical CO (toward the basal CO) slightly exacerbates—rather than mitigates—the closest contact with a H atom in the molecule, 2.64 Å. Note that the conformation and respective H−O distances in the calculated (gas phase) structure (Figure 4) are in remarkably good agreement with the crystallographically determined structure (Figure 3).

2.3.3. Nonlinearity of the Fe−C−O Angles. The bending of the apical CO ligand in **3** is remarkably well explained and characterized by the results and conclusions from Hoffmann's theoretical investigations (reported in 1974) of five-coordinate metal *nitrosyls*.[26] Although the M−C−O bending in **3** is clearly less than that found in typical bent nitrosyls, the qualitative similarities are sufficient to conclude with confidence that the same factors leading to bending in nitrosyls are responsible for the carbonyl bending in **3**. Applicable salient points made by Hoffman et al. in the context of nitrosyls include the following.[26]

(1) "The better the σ- or π-donating capability of the basal ligands, the more likely is the nitrosyl to bend." Accordingly, calculations on analogues of **3-SQP** with para-substituents on the pyridyl ring predict that the degree of apical Fe−C−O bending correlates with electron-donating ability as follows: H_2N (171.8°) > H (173.9°) > CH_2^+ (175.6°).

(2) "In a compound of the type $ML_2DA(NO)$, D = π-donor trans to A = π-acceptor, if the NO group bends in the DMA plane, then it should bend toward the acceptor." Accordingly the apical CO ligand is bent toward the basal CO.

(3) "A bent nitrosyl will move its nitrogen off the coordination axis in the direction of π-coordination, as indicated in [structure 5]." Hoffmann's graphic depiction of this is reproduced here. In accord with this prediction, the apical carbonyl carbon in **3** is closer to the PNP nitrogen (the atom from which it is bending away) than to the basal carbonyl carbon; the respective L−Fe−C angles are 101.6° and 105.8°. The difference between the analogous L−M−N angles is naturally slightly larger in the case of fully bent nitrosyls; for example, in the case of an archetypal bent nitrosyl compound, $IrCl_2(NO)(PPh_3)_2$, the respective angles are 89.3° and 100.5°.

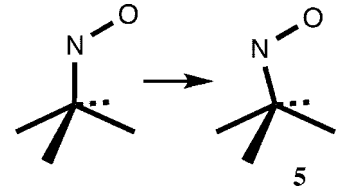

5

(4) "The nitrosyl is less likely to bend in the equatorial position of a trigonal bipyramid than in the apical site of a square pyramid." Accordingly, the apical carbonyl in **3** (and computationally, **3-SQP**) is more bent than the equatorial carbonyls of **4**[25] (or the calculated structure for **4**), cf. Table 4. (However, the carbonyls of **3-TBP** are computed to be slightly (~1°) more bent than the apical carbonyl in **3**.)

(5) "Nitrosyl groups in axial positions in a trigonal bipyramid and basal sites in a square pyramid prefer to be linearly coordinated." Although the basal carbonyl in **3** (or the calculated structure **3-SQP**) is not fully linear, this statement by Hoffmann, extrapolated to carbonyls, correctly predicts that the basal carbonyl of **3** is less bent than either the apical carbonyl of **3** or the equatorial carbonyls of **4**.

Finally, we note that Hoffmann's studies do not predict that bent nitrosyls in five-coordinate complexes are restricted to the apical position of SQP structures. It is noted, however, that the factors favoring bending would be greatest in that position, followed by the equatorial position of TBP structures and then by the basal position of SQP complexes. Only the axial position

(26) Hoffmann, R.; Chen, M. M. L.; Elian, M.; Rossi, A. R.; Mingos, D. M. P. *Inorg. Chem.* **1974**, *13*, 2666–2675.

of the TBP structure, among sites in the idealized geometries, affords no tendency toward M−N−O bending. Accordingly, from the X-ray data we find that the bending in complex **4** (174.8°)[25] is less than that for the apical position of **3** (171.9°), but greater than that of the basal carbonyl in **3** (176.7°).

Bent-carbonyl complexes are well precedented,[27−49] although, to our knowledge, this report represents the first examples that have been characterized by crystallographic and computational methods, thereby ruling out crystal-packing effects. While crystal structures have been reported with M−C−O angles more severely bent than in **3**,[28−32] to our knowledge all such structures show disorder,[31,32] high esd's for the M−C−O angle,[28,30,31] and/or anomalously short C−O bond lengths;[29] thus the significance of such reported angles is doubtful.[50]

We attribute the significant M−C−O bending in **3** to a combination of two characteristics of this complex. The first such characteristic is the highly electron-donating nature of the PNP ligand and the resulting very electron-rich nature of the Fe(0) center to which the carbonyls are bound. Bending, as Hoffmann et al. note for nitrosyls,[26] results in a net transfer of electron density from the metal to the nitrosyl. (This is of course consistent with the conventional formality of treating a bent nitrosyl as NO^- and linear nitrosyl as NO^+.) It is notable (though undoubtedly somewhat accidental) that the *average* bending of the two carbonyls is essentially identical in the X-ray structures of **3** and **4**. In the case of **3** however, steric effects result in the SQP coordination geometry (in the solid state and as the major solution isomer), somewhat unusual for d^8 five-coordinate complexes. Since apical nitrosyls (and presumably carbonyls) have the greatest tendency toward bending, the unusual SQP coordination geometry represents the second characteristic of **3** that results in the relatively extreme bending of one of the CO ligands.

2.3.4. Electronic Spectrum of 3. The excited-state calculations (simulated MeCN solution) predict strong electronic absorptions at $\lambda = 655$ nm (f = oscillator strength = 0.06) and 545 nm ($f = 0.04$) in **3-SQP** and at $\lambda = 563$ nm ($f = 0.12$) in **3-TBP** (cf. experimental $\lambda_{max} = 627$ nm in acetonitrile, presumably for a thermally equilibrated mixture of **3-SQP** and **3-TBP**). Examination of the transition amplitudes shows that these transitions are all metal−ligand charge transfer (MLCT) in character. The donor orbital in all three transitions is the HOMO of **3**, which is principally a metal d(π) orbital with some p character mixed in. The HOMO is oriented perpendicular to the P−Fe−P axis and interacts strongly with the π-type orbitals of the PNP ligand. The acceptor orbital for the long-wavelength transitions (655 nm in **3-SQP**; 563 nm in **3-TBP**) is the LUMO of **3**, a delocalized aromatic π^* orbital located exclusively on the PNP ligand with a substantial contribution from the pyridine N atom. The shorter wavelength transition in **3-SQP** (545 nm) terminates in a higher lying PNP π^* orbital. Good donor−acceptor overlap thus accounts for the substantial computed (and observed) intensity of these MLCT transitions.

The low transition energy of **3** (blue color) reflects the considerable electron richness of the Fe(0) center and, consequently, energetically high lying Fe[d(π)] orbital(s). Considering **4** as **3-TBP** in which the *t*-Bu groups have been replaced by less electron-donating *i*-Pr groups, a blue-shifted MLCT absorption band is anticipated. Indeed, the long-wavelength MLCT absorption in **4** is computed at $\lambda = 506$ nm ($f = 0.12$), a shift of more than 50 nm relative to **3-TBP** and in accord with the "red" color reported for crystalline **4**.[25]

3. Conclusions

Two unusual PNP complexes have been synthesized and fully characterized by spectroscopic and computational means. Complex **1**, (^{tBu}PNP)$FeCl_2$, also independently synthesized by Milstein, has unusually long iron−ligand bond distances. DFT calculations show that these are clearly attributable to its high-spin electronic structure, and in particular to occupancy of the strongly antibonding $d_{x^2-y^2}$ orbital. Complex **3**, (^{tBu}PNP)-$Fe(CO)_2$ has an unusual SQP structure in the solid state. However, in solution, **3-SQP** and **3-TBP** isomers are in equilibrium, with **3-SQP** favored. A SQP structure allows for some relief of steric crowding by providing an open space trans to the apical ligand. Consequently, the PNP ligand bends such that two *tert*-butyl groups can occupy that space, thereby reducing steric interactions with the carbonyl ligands.

Of particular interest, the apical Fe−C−O angle deviates significantly from linearity. Further analysis of this structure leads to the conclusion that CO responds qualitatively like NO to the same electronic factors that favor ligand bending. Since M−N−O bending transfers charge from metal to the ligand,

(27) There has been particular interest in bent metal carbonyls, and bent iron carbonyls in particular, in the context of hemoglobin and especially myoglobin. However such complexes are not closely related to the Fe(0) complex **3**, and any Fe−C−O bending is presumed to be due to factors in the environment of the CO ligand rather than any property intrinsic to the Fe−CO bonding. For lead references, see: (a) Spiro, T. G.; Kozlowski, P. M. *Acc. Chem. Res.* **2001**, *34*, 137–144. (b) Lian, T.; Locke, B.; Kitagawa, T.; Nagai, M.; Hochstrasser, R. M. *Biochemistry* **1993**, *32*, 5809–5814.

(28) Reisner, G. M.; Bernal, I.; Dobson, G. R. *J. Organomet. Chem.* **1978**, *157*, 23–39.

(29) Schumann, H.; Heisler, M.; Pickardt, J. *Chem. Ber.* **1977**, *110*, 1020–1026.

(30) Kreiter, C. G.; Wendt, G.; Sheldrick, W. S. *J. Organomet. Chem.* **1987**, *333*, 47–59.

(31) Rickard, C. E. F.; Roper, W. R.; Taylor, G. E.; Waters, J. M.; Wright, L. J. *J. Organomet. Chem.* **1990**, *389*, 375–388.

(32) Lin, J. T.; Sun, S.-S.; Wu, J. J.; Liaw, Y.-C.; Lin, K.-J. *J. Organomet. Chem.* **1996**, *517*, 217–226.

(33) Atwood, J. L.; Beveridge, K. A.; Bushnell, G. W.; Dixon, K. R.; Eadie, D. T. R. S. S.; Zaworotko, M. J. *Inorg. Chem.* **1984**, *23*, 4050–4057.

(34) Riley, P. E.; Davis, R. E.; Allison, N. T.; Jones, W. M. *Inorg. Chem.* **1982**, *21*, 1321–1328.

(35) Van Vuuren, P. J.; Fletterick, R. J. J. M.; Hughes, R. E. *J. Am. Chem. Soc.* **1971**, *93*, 4394–4399.

(36) Ellis, D. D.; Franken, A.; Jelliss, P. A.; Kautz, J. A.; Stone, F. G. A.; Yu, Y. *J. Chem. Soc., Dalton. Trans.* **2000**, 2509–2520.

(37) Dutta, D. K.; Woollins, J. D.; Slawin, A. M. Z.; Knonwar, D.; Das, P.; Sharma, M.; Bhattacharyya, P.; Aucott, S. M. *Dalton Trans.* **2003**, *13*, 2674–2679.

(38) Williams, G. M.; Rudisill, D. E.; Barnum, B. A.; Hardcastle, K.; Heyn, R. H.; Kozak, C. J.; McMillan, J. W. *J. Am. Chem. Soc.* **1990**, *112*, 205–215.

(39) Johnson, K. A.; Gladfelter, W. L. *J. Am. Chem. Soc.* **1991**, *113*, 5097–5099.

(40) Johnson, K. A.; Gladfelter, W. L. *Organometallics* **1992**, *11*, 2534–2542.

(41) Calderazzo, F.; Mazzi, U.; Pampaloni, G.; Roli, R.; Tisato, F.; Zanazzi, P. F. *Gazz. Chim. Ital.* **1989**, *119*, 241–247.

(42) Howard, J. A. K.; Jeffery, J. C.; Laguna, M.; Navarro, R.; Stone, F. G. A. *J. Chem. Soc., Chem. Commun.* **1979**, 1170–1171.

(43) Ooyama, D.; Tomon, T.; Tsuge, K.; Tanaka, K. *J. Organomet. Chem.* **2001**, *619*, 299–304.

(44) Bent, E. G.; Schaeffer, R.; Haltiwanger, C.; Norman, A. D. *J. Organomet. Chem.* **1989**, *364*, C25–C28.

(45) Denise, B.; Massoud, A.; Parlier, A.; Rudler, H.; Daran, J. C.; Vaissermann, J. C. A.; Patino, R.; Toscano, R. A. *J. Organomet. Chem.* **1990**, *386*, 51–62.

(46) Mague, J. T.; Johnson, M. P. *Organometallics* **1990**, *9*, 1254–1269.

(47) Liu, L.-K.; Sun, C.-H.; Yang, C.-Z.; Wen, Y.-S.; Wu, C.-F.; Shih, S.-Y.; Lin, K.-S. *Organometallics* **1992**, *11*, 972–976.

(48) Balch, A. I.; Noll, B. C.; Olmstead, M. M.; Toronto, D. V. *Inorg. Chem.* **1992**, *31*, 5226–5230.

(49) Yang, J.; Yin, J.; Abboud, K. A.; Jones, W. M. *Organometallics* **1994**, *13*, 971–978.

(50) We omit from this discussion bridging carbonyls or CO ligands that are interacting with any group extrinsic to the M−CO bond such as a nucleophile.

and considering the additional positive charge on NO, it is natural that bending would be much more common and much more pronounced for NO. The extent to which CO bending plays a role in the chemistry of M−CO complexes is unclear, but we propose that it merits consideration and further investigation. We have previously calculated that the TS for CO addition to $Ir(PR_3)_2(CO)X$ complexes (which is itself, formally, a five-coordinate SQP d^8 "complex") has a strongly bent (incipient) Ir−C−O bond.[51] More recently, it has been calculated that M−CO bending is required for addition of alkyl radicals to metal carbonyls (interestingly, this reaction is particularly favorable for five-coordinate d^8 carbonyls, and the transition state for addition to $Ru(CO)_5$ was found to be an SQP structure with methyl adding to a bent apical carbonyl).[52] We also speculate that bending of M−C−O angles might help alleviate buildup of charge in certain transition states, for example, TSs for associative ligand substitutions.

4. Experimental Section

All reactions were conducted under an argon atmosphere unless otherwise noted. All solvents were purchased as anhydrous from Aldrich and degassed with argon. NMR spectra were recorded on Varian 400 and 300 MHz spectrometers. ^{1}H NMR signals were calibrated using the residual proton peaks of the deuterated solvent. ^{31}P NMR signals are calibrated with an external reference, a capillary with a solution of *p*-xylene-d_{10} and PMe_3 (δ −62.4 ppm). Elemental analysis was performed by Robertson Microlit Laboratories. X-ray diffraction data were obtained from an oil-coated crystal mounted on a glass fiber. X-ray intensity measurements were made using a Bruker-AXS Smart APEX CCD diffractometer with graphite-monochromatized Mo Kα radiation at 100 K. Magnetic susceptibility measurements were obtained on a Quantum Design superconducting quantum interference device (SQUID) magnetometer (MPMS-XL). Electronic absorption data were collected using a Perkin-Elmer Lambda 40 UV−vis spectrometer. IR data were collected on an Avatar 360 FT-IR.

$^{t\mathrm{Bu}}$PNP. The synthesis was conducted according to the literature;[53] purification, however, was achieved by extracting the crude material with benzene, filtering, and removing the solvent. The same procedure was repeated using diethyl ether to obtain the product as white microcrystals (yield 44%).

($^{t\mathrm{Bu}}$PNP)FeCl$_2$ (1). $FeCl_2 \cdot 4H_2O$ (0.25 g, 1.26 mmol) was placed in a vial and dissolved in 5 mL of ethanol. In a separate vial, $^{t\mathrm{Bu}}$PNP (0.50 g, 1.26 mmol) was dissolved in 10 mL of benzene. The $^{t\mathrm{Bu}}$PNP solution was added to the $FeCl_2 \cdot 4H_2O$ solution, immediately resulting in an orange solution. The solvent was removed by vacuum to give a yellow solid. Ethanol (10 mL) was added to the solid, and the slurry was placed at −48 °C overnight. The solution was filtered to give yellow crystals that were washed with pentane (3 × 5 mL). Yield = 0.40 g (60%). ^{1}H NMR (300 MHz, CD_3CN): δ 54.9 (br, 2H, *m*-py), 18−14 (v br, 4H, CH_2), 10.1 (br, 36H, ^{t}Bu), −10.0 (br, 1H, *p*-py). Anal. Calcd for $FeP_2NCl_2C_{23}H_{43}$: C, 52.89; H, 8.29, N, 2.68; Cl, 13.58. Found: C, 52.01; H, 8.47; N, 2.50; Cl, 13.62.

($^{t\mathrm{Bu}}$PNP)FeHCl (2). ($^{t\mathrm{Bu}}$PNP)FeCl$_2$ (10.0 mg, 1.914×10^{-2} mmol) was placed in a vial and dissolved in 0.5 mL of acetonitrile to give a yellow solution. In a separate vial a solution of NEt_4BH_4 (10.0 mg, 6.892×10^{-2} mmol) in 0.5 mL of acetonitrile was made and added to the ($^{t\mathrm{Bu}}$PNP)FeCl$_2$ solution and left to stand at room temperature overnight. The resulting bright red solution was filtered to remove precipitates. ^{1}H NMR (300 MHz, CD_3CN): −13.623 (t, Fe-*H*, J_{P-H} = 58). ^{31}P NMR (121 MHz, CD_3CN): δ 102.7 (d, J_{P-H} = 51).

($^{t\mathrm{Bu}}$PNP)Fe(CO)$_2$ (3). Method 1: ($^{t\mathrm{Bu}}$PNP)FeCl$_2$ (20.0 mg, 0.0383 mmol) and $[Et_4N][BH_4]$ (25.3 mg, 0.153 mmol) were dissolved in 0.7 mL of CD_3CN and placed in a J. Young NMR tube. CO (1 atm) was added and the tube inverted three times to mix before being placed in an 2-propanol/ice bath overnight. The solution was filtered through a pipet with glass wool into a vial, and the solvent was slowly evaporated to give blue crystals suitable for X-ray diffraction (5.2 mg, 27%).

Method 2:[25] A 5% sodium amalgam was made and placed in a cuvette-bottomed Schlenk flask with a large head space that contained a magnetic stir bar. The flask was placed under 1 atm of CO. In the glovebox, a solution of ($^{t\mathrm{Bu}}$PNP)FeCl$_2$ in toluene was made. The solution was taken up by syringe and injected into the flask with CO. The solution was stirred vigorously overnight, resulting in the formation of a dark blue solution. Slow evaporation of the solvent led to the formation of a dark blue solid. ^{1}H NMR (400 MHz, toluene-d_8, room temperature): δ 6.29 (br, 2H, *m*-pyridine), 2.95 (broad, 4H, CH_2), 1.36 (br, 36H, *tert*-butyl). ^{1}H NMR (400 MHz, toluene-d_8,−80 °C): δ 6.50 (br, 1H, *p*-pyridine), 6.21 (br, 2H, *m*-pyridine), 2.79 (br, 4H, CH_2), 1.33 (br, 36H, *tert*-butyl). ^{31}P{^{1}H} NMR (121 MHz, toluene-d_8, room temperature): δ 123−119 (v br, ($^{t\mathrm{Bu}}$PNP)Fe(CO)$_2$), 76.18, 34.63 (free $^{t\mathrm{Bu}}$PNP). ^{31}P{^{1}H} NMR (121 MHz, toluene-d_8, −80 °C): δ 124.10, 78.52, 35.00 ($^{t\mathrm{Bu}}$PNP). IR (THF): ν_{CO} = 1870, 1846, 1819, 1797 cm^{-1}. Electronic absorption 627 nm (very broad, low intensity).

($^{t\mathrm{Bu}}$PNP)Fe(^{13}CO)$_2$. ^{1}H NMR (400 MHz, toluene-d_8, room temperature): δ 6.45 (br, 1H, *p*-pyridine), 6.27 (br, 2H, *m*-pyridine), 2.94 (br, 4H, CH_2), 1.34 (br, 36H, *tert*-butyl). ^{1}H NMR (400 MHz, toluene-d_8,−80 °C): δ 6.22 (br, 2H, *m*-pyridine), 2.71 (br, 4H, CH_2), 1.32 (br, 36H, *tert*-butyl). ^{31}P{^{1}H} NMR (162 MHz, toluene-d_8, room temperature): δ 122.15 (t, J_{P-C} = 19), 35.00 (free $^{t\mathrm{Bu}}$PNP). ^{31}P{^{1}H} NMR (162 MHz, toluene-d_8,−80 °C): δ 123.43 (br), 35.00 (free $^{t\mathrm{Bu}}$PNP). ^{13}C NMR NMR (101 MHz, toluene-d_8, room temperature): δ 230.65. ^{13}C NMR (101 MHz, toluene-d_8,−80 °C): δ 230.74 (t, J_{P-C} = 19). IR (THF): ν_{CO} = 1828, 1804, 1775, 1756 cm^{-1}.

5. Computational Details

Ground-state electronic structure calculations employed the DFT[54] method along with the PBE[55] exchange and correlation functionals. We used a relativistic 10-electron ECP and corresponding basis set (6s5p3d1f) for the Fe atom (SDD model);[56] all-electron, full double-ζ plus polarization function D95(d) basis sets for the second- and third-row elements C, N, O, P, and Cl;[57] and a split-valence 21G basis set for the hydrogen atoms.[58] Geometries of stationary points on the potential energy surfaces were fully optimized and characterized by normal-mode analysis. Standard thermodynamic corrections were made to convert the computed potential energies to free energies (G^o; T = 298 K, P = 1 atm).[59]

Electronic transition energies and moments (f = oscillator strength) were calculated using the TD-DFT formalism[60] and the

(51) Abu-Hasanayn, F.; Krogh-Jespersen, K.; Goldman, A. S. *J. Am. Chem. Soc.* **1994**, *116*, 5979–5980.
(52) Hasanayn, F.; Nsouli, N. H.; Al-Ayoubi, A.; Goldman, A. S. *J. Am. Chem. Soc.* **2008**, *130*, 511–521.
(53) Hermann, D.; Gandelman, M.; Rozenberg, H.; Shimon, L. J. W.; Milstein, D. *Organometallics* **2002**, *21*, 812–818.
(54) Parr, R. G.; Yang, W. Density-Functional Theory of Atoms and Molecules; University Press: Oxford, 1989.
(55) Perdew, J. P.; Burke, K.; Ernzerhof, M. *Phys. Rev. Lett.* **1996**, *77*, 3865.
(56) Dolg, M.; Wedig, U.; Stoll, H.; Preuss, H. *J. Chem. Phys.* **1987**, *86*, 866–872.
(57) Dunning, T. H. ; Hay, P. J. In *Modern Theoretical Chemistry*; Schaefer, H. F. I., Ed.; Plenum: New York, 1976; pp 1−28.
(58) Binkley, J. S.; Pople, J. A.; Hehre, W. J. *J. Am. Chem. Soc.* **1980**, *102*, 939–947.
(59) McQuarrie, D. A. Statistical Thermodynamics; Harper and Row: New York, 1973.
(60) Casida, M. E.; Jamorski, C.; Casida, K. C.; Salahub, D. R. *J. Chem. Phys.* **1998**, *108*, 4439.

B3LYP combination of functionals[61] along with the ECP and basis sets described above. To model the continuum solvent, we applied a self-consistent reaction field model, CPCM, with default THF or MeCN parameters, as appropriate.[62]

We have not truncated the experimental molecules for the computational studies; that is, the computationally demanding *t*-Bu groups were kept on the P atoms in complexes **1**−**3** and not replaced by smaller alkyl groups (e.g., Me). Small alkyl groups may capture most of the electronic effects imparted by the *t*-Bu groups actually employed in the experimental systems, but they obviously do not fully model the steric bulk of *t*-Bu groups.[63] Many of the interesting structural features discussed here would in fact not have been discovered if truncated phosphino-alkyl groups had been applied.

All calculations were executed using the GAUSSIAN03 series of computer programs.[64]

Acknowledgment. We thank Louis Whaley for assistance with the magnetic susceptibility measurements and Brian Regler for his help with the electronic absorption spectra. We also thank the DOE and NSF for financial support. E.M.P. thanks GAANN for a graduate fellowship.

Supporting Information Available: Structural data for ($^{t\text{Bu}}$PNP)$FeCl_2$ (**1**) and ($^{t\text{Bu}}$PNP)$Fe(CO)_2$ (**3**), infrared spectra of ($^{t\text{Bu}}$PNP)$Fe(CO)_2$ and ($^{t\text{Bu}}$PNP)$Fe(^{13}CO)_2$. Computational data, including optimized geometries, absolute energies, and electronic transition energies, for **1**, **2**, **2-MeCN**, **3-SQP**, **3-TBP**, ($^{i\text{Pr}}$PNP)$Fe(CO)_2$ (**4**), and the TS for **3-SQP/3-TBP** interconversion. Curie−Weiss plot for complex **1**. Complete ref 64. This material is available free of charge via the Internet at http://pubs.acs.org.

OM800425P

(61) (a) Becke, A. D. *J. Chem. Phys.* **1993**, *98*, 5648–5652. (b) Lee, C.; Yang, W.; Parr, R. G. *Phys. Rev. B* **1988**, *37*, 785.
(62) Barone, V.; Cossi, M. *J. Phys. Chem. A* **1998**, *102*, 1995–2001.
(63) Wullen, C. J. V. *Comput. Chem.* **1997**, *18*, 1985–1992.
(64) Frisch, M. J.; et al. *Gaussian 03*, Revision B.03; Gaussian, Inc.: Pittsburgh, PA, 2003. See Supporting Information for full reference to Gaussian 03.